A multi-objective optimization algorithm based on self-organizing maps applied to wireless power transfer systems.

Sami Barmada, Marco Raugi, Mauro Tucci

Dept. of Energy, Systems, Territory, and Construction Engineering

University of Pisa

Largo LucioLazzarino, 56122, Pisa, Italy

fax: +39 0502217333

sami.barmada@ing.unipi.it phone: +39 0502217312

marco.raugi@ing.unipi.it phone: +39 0502217325

mauro.tucci@ing.unipi.it phone: +39 0502217348

A multi-objective optimization algorithm based on self-organizing maps applied to wireless power transfer systems.

In this work a new multi-objective population based optimization algorithm is presented and tested. In this contribution the concepts of fast non-dominating sorting and density estimation using the crowding distance are used to create a multi objective optimization algorithm based on previous work, which is a single objective evolutionary optimization algorithm based on Self Organizing Maps (SOM). The SOM paradigm introduces a strong collaboration between neighbours solutions that improves exploitation. Furthermore, the representative power of the SOM enhances the exploration and diversification. A state of the art benchmark approach is used to evaluate the performance of the proposed algorithm, obtaining positive results. The test problem uses an analytical model of an inductively coupled wireless power transfer system (WPT). The objective is to optimize the WPT model characteristics in order to allow simultaneous data and power transfer between the coils. The WPT design approach uses more degrees of freedom than existing technics leading to a number of solutions where both the power signals and the data signal can coexist on the same physical channel achieving good figures of merit.

Keywords: self-organizing maps; evolutionary algorithms; multi-objective optimization, wireless power transfer systems, power-line communications.

Introduction

Multi-objective optimization algorithm

A large number of applications make use of multi-objective optimization (MOP) algorithms, as they allow to carry out difficult search and optimization problems. Evolutionary algorithms (EAs) and swarm intelligence are the main families of nature-inspired methods, that try to exploit the relation between optimization and biological evolution [1]. Examples of EAs are evolutionary programming (EP), genetic algorithms (GAs), evolution strategies (ESs), differential evolution (DE), genetic programming (GP). Swarm intelligence algorithms include particle swarm optimization (PSO), ant colony optimization (ACO), bacterial foraging optimization (BFO), bees algorithm. All of these methods have been developed both to perform single-objective global optimization and multi-objective optimization. Among multi-objective optimization approaches, the strategy proposed in [2], that is the non-dominated sorting genetic algorithm (NSGA-II), has gained a large popularity, mainly because of two main factors:

1. reduced complexity with respect to previous approaches;

2. it is straightforward to adapt population based single-objective optimization algorithms to perform multi-objective optimization.

In fact NSGA II was originally developed as a multi-objective GA, but many single objective evolutionary algorithms have been modified and adapted to perform MOP implementing the heuristics defined in NSGA-II. As an example[3] introduces a multi-objective PSO based on NSGA-II, and [4] proposes a multi-objective DE optimization based on NSGA-II.

In this work a new multi-objective real-parameter optimization algorithm is presented and analyzed, which is based on the global optimization algorithm introduced by the authors [5] – [7], and denoted as SOC-opt, Self-Organizing centroids optimization. The concepts of fast non-dominating sorting and density estimation using the crowding distance are used in this work to implement a MOP search algorithm based on SOC-opt.

The problem is the minimization of a number of objective functions, $F_i(\mathbf{x})$, $i = 1 \cdots N_f$, where $\left\{F_i : \Omega \subseteq \Re^n \to \Re\right\}$, $\mathbf{x} \in \Omega$, and Ω is the domain of the search.

The proposed algorithm is based on the self-organizing maps (SOM), [8] that are popular neural networks for unsupervised learning, clustering and data visualization. These methods in general have a strong explorative power, and the final centroids tend to be disposed in a predefined topological order.

In the proposed strategy, each cell of the SOM contains a centroid (or an individual) that searches for the Pareto optimal solutions. The global task is to track the Pareto optimal front, which is approximated by the set of non-dominated solutions found by all centroids in all generations. The movement of centroids is obtained using a discrete-time dynamical filter, and the choice of this filter is flexible. The resulting method is an heuristic optimization algorithm that uses some evolutionary computation mechanisms such as selection and mutation (perturbation). The algorithm tries to take advantage of the explorative power of the SOMs: the collaboration between neighboring centroids enhances exploitation, whereas centroids that are far form each other will explore different areas of the search space, improving exploration and preserving diversification.

Application problem: Wireless Power Transfer model

Wireless Power Transfer (WPT) with magnetically coupled resonators for recharging devices is nowadays attracting the attention of many researchers of both academic and industry worlds as an alternative to a wired connection [9]–[11]. The use of WPT for the recharging of electric or hybrid vehicles seems a promising potential application of such technology because of its high reliability in hostile environments which could cause cable deterioration (dust, chemicals, tough weather condition). In addition, such systems are also characterized by high efficiency and robustness and reach the power of some hundreds of Watts at a distance of a few tenth of centimeters. References [12] – [15] are a few examples of the applications of WPT to electric vehicles.

In the last years, power line communication (PLC) has gained widespread interest as a viable option for broadband communications. Commercial modems are, at the present time, capable of reaching speeds of 500 Mb/sec, by using communication protocols such as OFDM. Consequently, an increasing number of applications take advantage from the potential of the PLC technology. In particular, a significant field of application and research is the use of PLC to enable in-vehicle communications and networking, since modern vehicles are provided with a large number of devices and features that require data communication. The in-vehicles applications of PLC systems

have been investigated in recent years, and the many results [16] – [23] reveal the interest in the topic. The authors have developed new methods and tools for the analysis and modeling of PLC systems [24]; a first analysis of the PLC channel onboard a full Electric Vehicle has been presented in [25] by the authors while in [26] a feasibility study on the PLC for communication between the vehicle and the power grid (V2G) has been performed.

The study proposed in [26] should be seen under the Smart Grid point of view, in which electric (or hybrid) vehicles play an important role as energy storage devices and PLC communication is probably the key communication technology.

This leads to the following consideration: from one side we are going to the direction of considering power/data (cabled) transmission between grid and vehicles as fundamental for the Smart Grid management, on the other side WPT technology is cutting the cable between vehicles and grid.

The performances of the proposed multi-objective optimization algorithm are tested on a specific problem characterized by the need of two specific (and colliding) objectives. In particular the authors have recently proposed a Wireless Power Transfer (WPT) system, based on non radiative magnetic resonance coils, integrated with a Power Line Communication (PLC) system, with the aim of transmitting both power and data through a wireless link [27-28]. The latter works are based on the observation that the broadband frequency response of near-field WPT systems working in the MHz range is similar to the frequency response of typical PLC channels. Possibly, the attenuation is higher in PLC channels. This new perspective is a crucial idea of the application developed in this work, as it allows us to use the frequency range that is not used for power transmission as a parallel data communication channel. In particular, the idea is to apply the multicarrier PLC technology as an additive communication signal.

We also believe that the automatic WPT optimization approach developed in this work gives some new insights with respect to the existing approaches for optimal WPT design [29]. For instance, we find a large number of different feasible solutions by removing the hypothesis that the transmitting and receiving circuits share the same resonance frequency. This occurs because we use more degrees of freedom (17 independent parameters), and we are searching design solutions that exhibit the following two properties:

3. the first goal is that some frequency exists where the WPT frequency response, or the energy efficiency, has a peak value close to one (as we use the frequency where this occurs as the carrier for power transmission),

4. the second goal is that the average channel amplitude in the broadband frequency range is maximum (as we use the whole band from 2MHz to 30 MHZ for data communication).

In general, existing approaches take into account only the first property, as WPT requires a resonance peak to work efficiently. The reason of the second property is that we use the channel for data communication in the frequency intervals not used for power transmission, and PLC modems (as any other communication system) use a wide frequency band in order to achieve a reasonable channel capacity (in terms of bit rate). For this reason, a secondary objective is to determine the maximum theoretic capacity of the data channel. An experimental prototype is under construction, and the real system includes couplers and filters that have the task of isolating the data channel from the power signal. In this work, we do not consider such further equipment, which add

more attenuation to the signal path, so the channel capacities estimated in this work should be considered as an upper bound.

Simultaneous power and data transmission is more common in the communities dedicated to far-field WPT systems, antennas and RFIDs [30], [31]. To the best of the author's knowledge, the use of a near-field WPT system for data transmission in the MHz range is less common, as well as the straightforward application of the existing PLC technology in parallel with the power transmission, as an additive communication signal. In particular, the PLC technology uses OFDM with hundreds, or thousands, of carriers, allowing fast data rates also in the presence of high attenuations and frequency selective channels, in the range form 2MHz to 30 MHz. The WPT channel is selective and narrow band in the frequency range around the peak resonance frequency, but considering the broadband frequency range, attenuations are compatible with the PLC modem technologies. Moreover, the PLC modems automatically exclude the frequencies where the signal to noise ratio (SNR) is low. Consequently, the frequencies around the power signal carrier will not be used for data communication. A contribution that is relatively close to our work is possibly [32], that develops a communication system for near-field WPT, and, in contrast to our proposal, it uses load modulation, and does not consider the use of an additive multicarrier communication signal.

In order to analyse the performance of the proposed optimization algorithm, the optimization of an analytical WPT model is used as a benchmark problem to compare the results of other state of the art multi-objective approaches, in particular NSGA-II approach. The results show that the proposed scheme, which is denote as SOC-MOP (Self Organizing Centroids Multi-Objective Optimization) is competitive with one of the most efficient multi-objective optimization algorithm. Regarding the design application, using the proposed approach we can define efficiently and accurately the WPT system characteristics, in terms of lumped parameters of the equivalent electric circuits of the four coils, taking into account both objectives and guide the designer to make choices accordingly.

Optimization Algorithm description

This section introduces the new algorithm for multi-objective optimization, denoted as SOC-MOP, which uses some of the concepts that define the SOC-opt algorithm. For more details regarding the single objective global optimization algorithm SOC-opt please see [5] – [7].

The proposed algorithm is constituted by two main elements:

- a grid of P cells containing a centroid vector,
- an external population of P solution points.

The cell behaves as an input-output model, where points from the external population represent the input and the centroid of the cell represents the output. The cells contain a memory of past input and output points, and the input-output relationship is guided by a linear dynamical filter action. The output centroid of each cell represents a moving agent in the solution space and it is used to generate new solutions of the external population by perturbation and selection. In particular, all the output centroids are first perturbed, in order to generate a new population of P individuals, which is then compared with the old population by using fast non dominated sorting. A new population of P solutions is then selected and presented as input to the grid of cells. In the following we first describe the cell model and then the steps to update the external population.

Cell model

The main element of the SOC-MOP consists in a number P of cells arranged in a two dimensional grid with a fixed topology, typically hexagonal. Each cell is identified by an index $i = 1 \cdots P$, and a distance metric is defined between each couple of cells $d(i, j)$, $i, j = 1 \cdots P$. Each cell is associated to a centroid, or individual, $\mathbf{q}^i \in \Re^n$, lying in the solution space. At each iteration the centroid moves towards a vector $\mathbf{r}^i \in \Re^n$, that represents a good possible solution found by the algorithm. The centroids movement is guided by a linear discrete time low pass dynamical filter of order *N*. In order to implement the filter action, each cell N contains two sets of vectors, denoted as memory vectors, $\mathbf{q}_j^i \in \Re^n$, and $\mathbf{r}_j^i \in \Re^n$, $j = 1 \cdots N$. The memory vectors $\mathbf{q}_j^i$, $\mathbf{r}_j^i$ take trace of the past N values of the centroid and of the input vector of the cell *i* respectively. Actually, we do not need to store the centroid position $\mathbf{q}^i$, since by definition it can be obtained, at each iteration step $t = 1 \cdots T_{MAX}$, by the following linear combination of the memory vectors:

$$\mathbf{q}^i(t) = \sum_{j=1}^{N} b_j \mathbf{r}_j^i(t) + a_j \mathbf{q}_j^i(t). \tag{1}$$

If we define the memory matrices $\mathbf{R}^i = \left[\mathbf{r}_1^i, \cdots \mathbf{r}_N^i\right]$ and $\mathbf{Q}^i = \left[\mathbf{q}_1^i, \cdots \mathbf{q}_N^i\right]$ $i = 1 \cdots P$, equation (1) can be expressed as

$$\mathbf{q}^i(t) = \left[\mathbf{R}^i(t) \vdots \mathbf{Q}^i(t)\right] \begin{pmatrix} \mathbf{b} \\ \mathbf{a} \end{pmatrix}, \tag{2}$$

where $\mathbf{b} = [b_1, \cdots, b_N]^T$, $\mathbf{a} = [a_1, \cdots, a_N]^T$ are the vectors containing the filter coefficients.

When a new input vector $\mathbf{r}^i(t)$ is presented to the cell, the memory vectors of the cell are updated as follows:

$$\begin{aligned} \mathbf{R}^i(t+1) &= \mathbf{R}^i(t) + h_{ki}(t)\left[\mathbf{R}_+^i(t) - \mathbf{R}^i(t)\right], \\ \mathbf{Q}^i(t+1) &= \mathbf{Q}^i(t) + h_{ki}(t)\left[\mathbf{Q}_+^i(t) - \mathbf{Q}^i(t)\right], \end{aligned} \tag{3}$$

where

$$\begin{aligned} \mathbf{R}_+^i(t) &= \left[\mathbf{r}^i(t), \mathbf{r}_1^i(t), \cdots \mathbf{r}_{N-1}^i(t)\right], \\ \mathbf{Q}_+^i(t) &= \left[\mathbf{q}^i(t), \mathbf{q}_1^i(t), \cdots \mathbf{q}_{N-1}^i(t)\right], \end{aligned} \tag{4}$$

and $h_{ki}(t) \in [0,1]$ is a neighborhood function defined later. Equation (4) performs a one step time shift of the memory vectors, while (3) takes into account neighborhood collaboration, i.e. the cell memory substantially updates only if the neighborhood function assumes high values. Equations (1), (3) and (4) can be interpreted as an implementation of a linear, time invariant, discrete time filter of order N, which has the following transfer function:

$$G(z) = \frac{b_1 z^{N-1} + \cdots + b_N}{z^N - a_1 z^{N-1} - a_2 z^{N-2} \cdots - a_N}, \tag{5}$$

which defined using the Z-Transform formalism. The coefficients $\mathbf{b} = [b_1, \cdots, b_N]^T$ and $\mathbf{a} = [a_1, \cdots, a_N]^T$ are fixed and define the particular filtering action between the input sequence and output sequence.

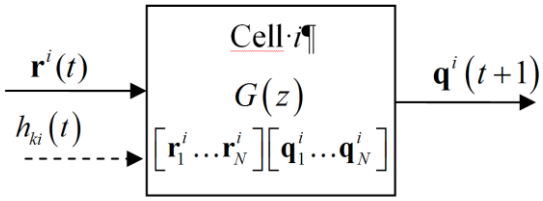

Figure 1.Input-output model of the cell *i*.

After the presentation of the new input and the memory update, the new output $\mathbf{q}^i(t+1)$ is obtained by (2), that substituting (4c) and (4d) gives:

$$\mathbf{q}^i(t+1) = \mathbf{q}^i(t) + h_{ki}(t)\left(\mathbf{q}_+^i(t) - \mathbf{q}^i(t)\right), \quad i = 1 \cdots P \tag{6}$$

where $\mathbf{q}_+^i(t) = \left[\mathbf{R}_+^i(t) \vdots \mathbf{Q}_+^i(t)\right]\begin{pmatrix}\mathbf{b}\\ \mathbf{a}\end{pmatrix}$.Then, at each iteration step the centroid moves towards $\mathbf{q}_+^i(t)$.If the filter $G(z)$ is low pass with unitary static gain, i.e. it is a follower filter, the centroid also tends to move in the direction of the input pattern $\mathbf{r}^i(t)$.

Figure 1 summarizes the input-output behaviour of a cell: at each iteration step it receives an input pattern $\mathbf{r}^i(t)$ and it produces an output $\mathbf{q}^i(t+1)$ as in (6), which also depends from a neighborhood function $h_{ki}(t)$. If $h_{ki}(t)$ has values near to 1 then the centroids performs one step of the filter dynamics and it moves towards the input, if the value of $h_{ki}(t)$ is near zero the centroid position remains unchanged, while for intermediate values of $h_{ki}(t)$ the centroids performs an intermediate step.

External population

A population of *P* individuals $\mathbf{t}^i \in \Re^n \; i = 1 \cdots P$ is considered lying outside of the grid of cells. The values of the objectives functions are known for all the solution points $\mathbf{t}^i$ of the external population, that also contain the best approximation of the Pareto front found by the algorithm. Note that the index *i* in $\mathbf{t}^i$ is not related to the cell indexing of the grid. However each solution $\mathbf{t}^i \; i = 1 \cdots P$ take trace of the cell it was generated from and it is shown by a second index $k \in \{1 \cdots P\}$: $\mathbf{t}^{i,k}$. The cell index *k* has values in the range 1...*P*, and different solutions $\mathbf{t}^i$ may have been generated from the same cell *k*. At each iteration the external population is merged with anew population, obtained perturbing the centroids, in order to search new non dominated solutions.

Centroid perturbation

All the nature inspired optimization techniques are based either on the concept of mutation or on the similarity with nature based processes characterized by interaction between different entities. In the proposed model each cell represents an individual that searches in an exclusive region of the solution space limited by neighboring cells. To obtain this we define a function $neigh(i)$ that returns the index of one cell belonging to the neighborhood of the cell i (the choice of the neighborhood cell is made a-priori in

the fixed grid). The distance between the centroid $\mathbf{q}^i$ and the neighbor $\mathbf{q}^{neigh(i)}$ is used to determine the range of the perturbation of the cell i .Given the output centroid $\mathbf{q}^i(t)$ of the cell *i* at the iteration *t*, the new *offspring* is generated by the following perturbation:

$$\mathbf{p}^i(t) = \mathbf{q}^i(t) + \delta^i(t), \tag{7}$$

in which $\mathbf{p}^i(t)$ is a perturbed centroid, obtained with the addition of a random perturbation $\boldsymbol{\delta}^i(t-1)$ whose components are uniformly distributed in $\left[-d_{neigh}, d_{neigh}\right]$, where $d_{neigh} = \left\|\mathbf{c}^i(t) - \mathbf{c}^{neigh(i)}(t)\right\|$. At this point all the objective functions are calculated in each perturbed point according to $F_j\left(\mathbf{p}^i(t)\right)$, $j = 1 \cdots N_f$.

Generation of the new external population

After the centroid perturbation we have two populations of *P* individuals where the objective functions values are known: the offspring (child) population $\mathbf{p}^i(t)$, $i = 1 \cdots P$, where *i* represents a cell index, and the old (parent) population $\mathbf{t}^{j,k}(t)$, $j = 1 \cdots P,\ k \in \{1 \cdots P\}$. The two populations are first combined obtaining a population of 2*P*solutions,and then ordered using the fast non dominated sorting approach as used in NSGA II, [2] .By comparing the combined 2*P*solutions for non-domination relationships, the entire population will be sorted in different non-domination levels. This process can be illustrated as follows: first the entire population is sorted into two sets, the non-dominated set, called Front 1, and the remaining dominated set. To obtain the next front, we temporarily remove Front 1 from the population, then find the non-dominated solutions of the remaining population, which is Front 2. Then again we remove Front 2 as well, in order to identify the non-dominated solutions of the next level. This procedure continues until all solutions in the population are classified into different non-dominated front levels. Following the NSGA-II approach, points inside the same front level are again sorted according to descending values of the crowding distance, [2].

Now we create the new external population $\mathbf{t}^{j,k}(t+1)$, of P individuals from the combined 2P population, by selecting points from fronts in ascending order(e.g., first from Front 1, then Front 2, etc,), until *P* points $\mathbf{t}^{j,k}(t+1)$, are selected, $j = 1 \cdots P$.Then, we are discarding the remaining *P* points, maintaining the *P* solutions nearest to the best approximation of the true Pareto front, which is Front 1. Note that for each selected point $\mathbf{t}^{j,k}(t+1)$, the cell index information *k* can be retrieved, both in the case that the selected point is child $\mathbf{p}^i(t)$ or a parent $\mathbf{t}^{j,k}(t)$. The final new population $\mathbf{t}^{j,k}(t+1)$, for $j = 1 \cdots P.$ is ordered for increasing front levels and, inside the same front, for decreasing crowding distance.

Input patterns to the cells and neighborhood function

At this point the new population is used as input for the cells of the fixed grid. In particular the input to cell *i* is as follows:

$$\mathbf{r}^i(t) = \mathbf{t}^{i,k}(t+1). \tag{8}$$

The cell index is now used to associate the input of cell *i* with the ith point of the external population. In this manner the first cells of the grid will always receive inputs from the Front 1. The cell index *k* contained in $\mathbf{t}^{i,k}(t+1)$ is used to determine the neighborhood function, which is defined by the Gaussian kernel:

$$h_{ki}(t) = \exp\left(-\frac{d(k,i)^2}{2\sigma^2}\right), \tag{9}$$

where σ represents the width of the neighborhood in the fixed grid. Then the strength of the centroid update $\mathbf{q}^i$ in (6) depends on the distance in the fixed grid between the cell *i* and the cell *k* from which the input pattern $\mathbf{t}^{i,k}$ was generated in the previous generations. In this way the centroid will be substantially updated if the distance $d(k,i)$ is small with respect to σ, then mainly if *k* and *i* coincide, or if they are adjacent cells. The neighborhood width σ is fixed so that the function $h_{ki}(t) =$ is negligible for second order neighbors in the grid.

Initialization and algorithm summary

At the first generation $t = 0$ all the cell memory and the external population need to be initialized. The centroids positions $\mathbf{q}^i(0)$ of each cell are defined randomly and the memory vectors are initialized as $\mathbf{r}_j^i(0) = \mathbf{q}_j^i(0) = \mathbf{q}^i(0)$, $j = 1 \cdots N$, $i = 1 \cdots P$. With this choice the relationship between the centroid and the memory vectors holds $\mathbf{q}^i(0) = \sum_{j=1}^{N} b_j \mathbf{r}_j^i(0) + a_j \mathbf{q}_j^i(0)$, because the filter coefficients are always selected with unitary sum, i.e. unitary static gain of the filter. At $t = 0$ the external population points are initially coincident with the centroids $\mathbf{t}^{i,i}(0) = \mathbf{q}^i(0)$, and their objective functions values are straightforwardly calculated as $F^j\left(\mathbf{t}^{i,i}(0)\right)$, $j = 1 \cdots N_f$,

After the initialization, the algorithm continue as follows for $t = 0 \cdots T_{\max}$:

1. perform the perturbation of the centroids $\mathbf{q}^i(t)$ to generate the child population $\mathbf{p}^i(t)$, $i = 1 \cdots P$, using equation (7).
2. Calculate the objective functions in each point of the child population $\mathbf{p}^i(t)$.
3. Combine the child population $\mathbf{p}^i(t)$ and the external population $\mathbf{t}^{i,k}(t)$ and perform the fast non dominated sorting of the combined population, also sorting points in the same fronts using the crowding distance.
4. Then select the first *P* points from the sorted combined population, obtaining the new external population $\mathbf{t}^{i,k}(t+1)$, $i = 1 \cdots P$.
5. Use the points of the new external population to define both the input points for the grid cells as $\mathbf{r}^i(t) = \mathbf{t}^{i,k}(t+1)$, and the neighborhood function as in equation (9).
6. Calculate the new centroid position $\mathbf{q}^i(t+1)$ using equation (6).
7. Put $t = t + 1$ and stop the algorithm if $t > T_{\max}$, or another stop criterion is matched. Otherwise return to step 1.

When the algorithm ends the Font 1 contained in the external population $\mathbf{t}^{i,k}(t)$ represents the final approximation of the true Pareto front.

The proposed algorithm is a framework that accepts a number of different configurations. For example the movement of the centroid is implemented by a discrete filter of order *N*, so that each centroid has a certain inertia, or activity, to track its input, depending on the particular choice of the filter, which can be more or less predictive.

Moreover the topology between the cells can be created in the input space following the Neural Gas paradigm instead of the SOM paradigm. Other variants of the proposed method can be defined using a different definition of the random perturbation $\boldsymbol{\delta}^i(t-1)$ in (7), for instance the random distribution can be chosen as Gaussian, while the amplitude of $\boldsymbol{\delta}^i(t-1)$ can be chosen as proportional to the distance between the centroid and the global best solution.

Constrains handling

A set of constraints for the search space is considered by defining maximum and minimum values for each optimization variable. These are direct constraints on the solution vector which are imposed in the initialization step and in the perturbation step (7). If an element of the randomly perturbed vector falls outside of the allowed interval, it is forced to a new random value that lies within the interval.

Parameters selection

The proposed method is characterized by some parameters to be selected. One of the parameters involved in the method is σ, the width of the neighborhood in the fixed spatial arrangement of the cells. If an hexagonal arrangement is used, the Euclidean distance between two adjacent cells is usually chosen to be 1, then σ is typically chosen so that the neighborhood include the first order and second order neighbors. For instance by choosing $\sigma_\lambda = 3$ the neighborhood function is negligible for third order neighbors.

Regarding space memory requirements, it increases linearly with the filter order. Acceptable space is required using a discrete filter with low order as 1, 2 or 3. Using a filter of order 1, the centroid update in (6) yields exactly the classic SOM update, as defined by [6]. In the context of the classic SOM use, In [5]it is shown that that a second order alpha-beta $G_{\alpha\beta}(z)$ predictive filter has good tracking capabilities. The discrete time transfer function $G_{\alpha\beta}(z)$ is the following:

$$G_{\alpha\beta}(z) = \frac{\alpha z + \beta - \alpha}{z^2 + (\beta + \alpha - 2)z + (1-\alpha)}. \tag{10}$$

The filter is univocally defined choosing the normalized cut off frequency, a parameter that is between zero and one. A cut-off frequency of 0.6 is selected for the following simulations.

Application example: WPT model optimization.

Lumped circuit WPT system model

Based on the observation that in most of the proposed WPT implementations the frequency operating point is in the MHz range, which is located inside the frequency range used by the Homeplug 2.0 standard for wide band PLC modems, the authors proposed in [27] a feasibility study of coupled WPT – PLC system, in which a PLC communication system is embedded in a WPT system. [27] presents a simple evaluation of the channel capacity for PLC using the Shannon law of a WPT system modeled by the well known equivalent circuit model. In addition, a block diagram of the whole system with the necessary electronic circuitry is introduced.

The equivalent circuit of a WPT system used in [27] and in this paper is shown in Fig. 2, where the magnetically coupled resonator system is represented by a lumped circuit element system composed by four resonant circuits, magnetically linked by coupling coefficients.

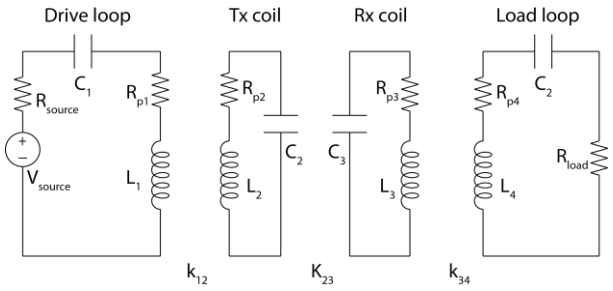

Figure 2. Lumped equivalent circuit of a WPT system

The high frequency generator (with its output impedance R_{source}) excites the drive loop which can be modeled as an inductor L_1 with parasitic resistance R_{p1} and a capacitor C_1 which makes the drive loop resonant at the frequency of interest. The drive loop is coupled to the transmitter coil, which is realized as a multi turn inductor, modeled by the inductance L_2 and parasitic resistance R_{p2}, while C_2 plays the same role as the capacitance C_1 for the drive loop. The coupling coefficient K_{12} connects the two inductors and is in general a fixed parameter since the drive loop and the transmitter coil are often built in the same device; the same description holds for the receiver coil and the load loop. The coupling coefficient K_{23}, between the transmitter and received coil, strictly depends on the distance between the coils and suffers of distance uncertainty, and misalignment.

Table I. Circuit parameters.

Parameter	**Value**
R_{Source}, R_{Load}	50Ω
L_1, L_4	1.0μH
C_1, C_4	235pF
R_{p1}, R_{p4}	0.25Ω
K_{12}, K_{34}	0.10
L_2, L_3	20.0μH
C_2, C_3	12.6 pF
R_{p2}, R_{p3}	1.0Ω
K_{23}	0.0001 to 0.3
f0	10MHz

The authors have considered the real system setup proposed in [33], in which the parameters for the components of the equivalent circuit shown in Fig.1 are given in Table I.

As for the channel capacity for PLC communication we can refer to the Shannon - Harltey approach: the signal sent from the transmitter is filtered by the channel transfer's function, which is in general selective, and reaches the receiver together with

the noise which, in this case, is mainly produced by the signal generator and RF amplifier. The following Shannon–Hartley law can be used

$$C = \int_0^B \log_2 \left(1 + \frac{S(f)}{N(f)} \right) df \tag{11}$$

in which C is the channel capacity in bits per second, B is the bandwidth of the channel, $S(f)$ is the signal power spectrum, $N(f)$ is the noise power spectrum and f is frequency. As for the channel capacity objective, the following assumptions are made: both the injected power spectrum $S_I(f) = S_I$, and the noise power spectrum $N(f) = N$, are frequency independent, and the noise is considered as additive white Gaussian noise at the receiver. The signal to noise ratio is then defined as $SNR = S_I / N$, and the received power spectrum can be expressed as a function of the injected power spectrum and the transfer function, according to $S(f) = |H(f)|^2 S_I$. Under these assumptions (11) can be rewritten as

$$C(SNR) = \int_0^B \log_2 \left(1 + |H(f)|^2 SNR \right) df \ , \tag{12}$$

where the capacity is defined as a function of the SNR value.

As a matter of fact maximum power can be delivered under a resonance condition, but resonances are by nature narrowband, hence not suitable for data transmission which is limited by bandwidth. This leads to a tradeoff in the design process of such system. In [33] the evaluation of the channel capacity is performed using (12) for different values of the coupling parameter K_{23} (which is an indirect measure between the charging device and the vehicle) and the results show how over coupled systems (hence presenting the frequency splitting phenomena) are better in terms of capacity since they are characterized by a higher band.

In order to design a better system that could carry both power and information in an efficient way, the above mentioned optimization algorithm is used. The authors investigate two different aspects of the power transfer: power transfer efficiency and energy efficiency. Analytical solution of the circuit leads to the following equations

$$\begin{aligned}
&\frac{\dot{V}_L}{\dot{V}_S} = \frac{j\omega^3 K_{12} K_{23} K_{34} L_2 L_3 \sqrt{L_1 L_4} R_{load}}{\left(K_{12}^2 K_{34}^2 L_1 L_2 L_3 L_4 \omega^4 + \bar{Z}_1 \bar{Z}_2 \bar{Z}_3 \bar{Z}_4 + \omega^2 \left(K_{12}^2 L_1 L_2 \bar{Z}_3 \bar{Z}_4 + K_{23}^2 L_2 L_3 \bar{Z}_1 \bar{Z}_4 + K_{34}^2 L_3 L_4 \bar{Z}_1 \bar{Z}_2 \right) \right)} \\
&\bar{Z}_1 = R_{p1} + R_{source} + j\omega L_1 - \frac{j}{\omega C_1} \\
&\bar{Z}_2 = R_{p2} + j\omega L_2 - \frac{j}{\omega C_2} \\
&\bar{Z}_3 = R_{p3} + j\omega L_3 - \frac{j}{\omega C_3} \\
&\bar{Z}_4 = R_{p4} + R_{load} + j\omega L_4 - \frac{j}{\omega C_4}
\end{aligned} \tag{13}$$

while the current generated by the source is

$$\dot{I}_{source} = \frac{\dot{V}_L}{\dot{Z}_1 + \left(\omega^2 K_{12}^2 L_1 L_2 \Big/ \dot{Z}_2 + \frac{\omega^2 K_{23}^2 L_2 L_3}{\dot{Z}_3 + \frac{\omega^2 K_{34}^2 L_3 L_4}{\dot{Z}_4}} \right)} \tag{14}$$

As known, maximum power transfer is related to the scattering parameter S_{21} according to (12)

$$S_{21} = 2\frac{V_L}{V_S}\sqrt{\frac{R_{source}}{R_{load}}} \tag{15}$$

On the other hand energy efficiency is evaluated as

$$\eta = \frac{R_{load} I_{load}^2}{\sum_j R_i I_i^2} = \frac{R_{load} I_{load}^2}{\Re e\left(\dot{V}_{source} \cdot \dot{I}_{source}^*\right)} \tag{16}$$

in which I_i and R_i respectively are the currents and resistances in each loop. As a rule of thumb, taking into account (16) should be necessary when mid – and – high – power applications, while (15) is suitable for relatively low power applications.

Optimization of the WPT model for data and power transfer

In this work we developed an automatic WPT multi-objective optimization approach, where we find a large number of different feasible solutions: all the solutions on the Pareto front are equally optimal. We consider the 17 circuit parameters shown in table II, which define the lumped equivalent circuit in Fig. 2, and we remove the hypothesis that the transmitting and receiving circuits share the same resonance frequency. The resonance frequencies of the two circuits will be determined automatically by the optimization process.

Table II. Seventeen design parameters.

Optimization design Parameters
R_{Source}, R_{Load}
L_1, L_4, L_2, L_3
C_1, C_4, C_2, C_3
R_{p1}, R_{p4}, R_{p2}, R_{p3}
K_{12}, K_{34}, K_{23}

The multi-objective optimization is performed by taking into account the following objective functions, which depend on the parameters shown in Table II.

1. Maximize the absolute value of (15) or (16) in the frequency range of 2-30MHz. The first goal is that some frequency exists where the WPT frequency response, or the energy efficiency, has a maximum value close to one (as we use the frequency where this occurs as the carrier for power transmission). We consider both (15) and (16) in order to show how different power objectives lead to different system design criteria.

2. Maximize the mean value of (12) (averaging for SNR values in the range 1db-20db). The second goal is that the average channel capacity C in the broadband frequency range is maximum (as we use the whole band from 2MHz to 30 MHZ for data communication).

In general, existing approaches take into account only the first property, as WPT requires a resonance peak to work efficiently. The reason of the second property is that we use the channel for data communication in the frequency intervals not used for power transmission, and PLC modems (as any other communication system) use a wide frequency band in order to achieve a reasonable channel capacity (in terms of bit rate). For this reason, a secondary objective is to determine the maximum theoretic capacity of the data channel.

Being a preliminary study (a prototype is under construction) the constraints on the parameters have been set based on physical considerations: coupling coefficients in the range [0.1, 0.5] and the maximum value of each lumped parameter is fixed as 10 times the value the corresponding parameters in Table I. The capacitances and inductances of each loop/coil are not constrained to a particular resonant frequency, in this way the best operating frequency for the power transfer performances will be decided based on the results. Furthermore, a constraint on the frequency location of the peak resonance can be introduced as a nonlinear constraint of the optimization algorithm, so that the peak of the response is inside an ISM (Industrial, Scientific and Medical) band.

A schematic of the proposed integration between PLC and WPT, that uses an ISM band of 6.78 MHz, is shown in Figure 3. The system allows for unidirectional power transfer and bidirectional communication. The bandstop and bandpass filters. with center frequency at 6.78 MHz. are designed as narroband filters, and their purpose is to allow electric coupling between the radio frequency power signal and the low power broadband communication signal.

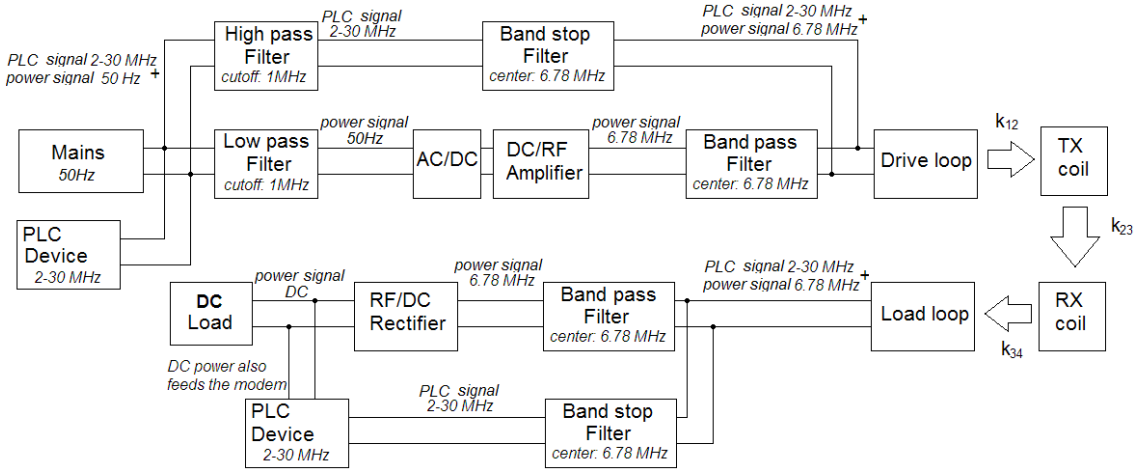

Figure 3. Schematic of the proposed PLC and WPT integrated system.

Results for optimization of S_{21} and C

Figures 4 and 5 show the results obtained by simultaneously optimizing S_{21} and the channel capacity; in particular 70 different optimal results (points in the Pareto front) have been obtained and, as it is easy to verify, all the curves are similar to each other and no big differences in terms of the channel capacity can be found. Figure 6 shows S_{21} and the energy efficiency demonstrating that when maximum power transfer

efficiency is reached the energy efficiency is approximately 0.5. The solution shown in figure 6 is one solution among all of the optimal solutions shown in figure 4, and it has been selected so that the peak of S_{21} occurs in the ISM frequency band around 6.78MHz. The obtained optimal parameters of the solution shown in figure 6 are presented in table III.

Table III. One optimal solution of the Pareto front, frequency peak is at 6.78MHz.

Parameter	**Value**
R_{Source},	37.4 Ω
R_{Load}	126.6
L_1 L_4	2.66 µH
L_4	4.80 µH
C_1	714 pF
C_4	566 pF
R_{p1}	2.38 Ω
R_{p4}	2.93 Ω
K_{12}, K_{34}	0.499
L_2	92.7 µH
L_3	41.2 µH
C_2	22.5 pF
C_3	48.6 pF
R_{p2}	4.62 Ω
R_{p3}	3.24 Ω
K_{23}	0.499

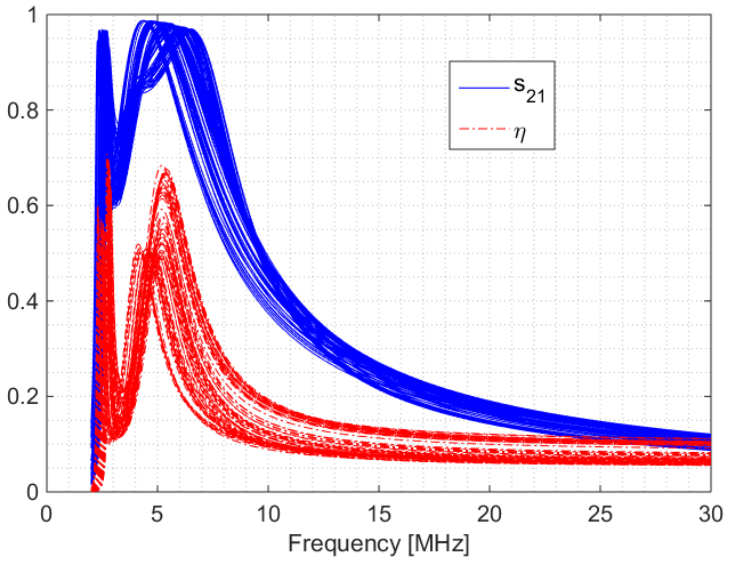

Figure 4. All of the optimal S_{21} and η solution curves with multi-objective optimization performed on S_{21} and C

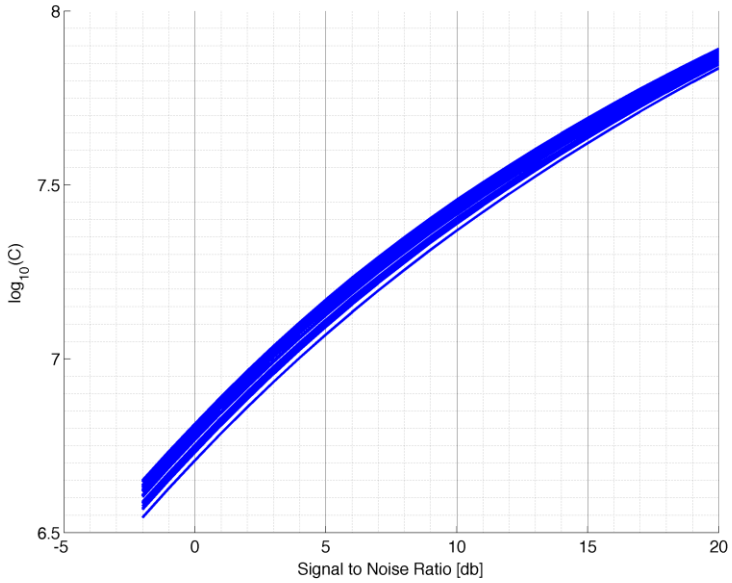

Figure 5. *C* curves with multi-objective optimization performed on S_{21} and *C*

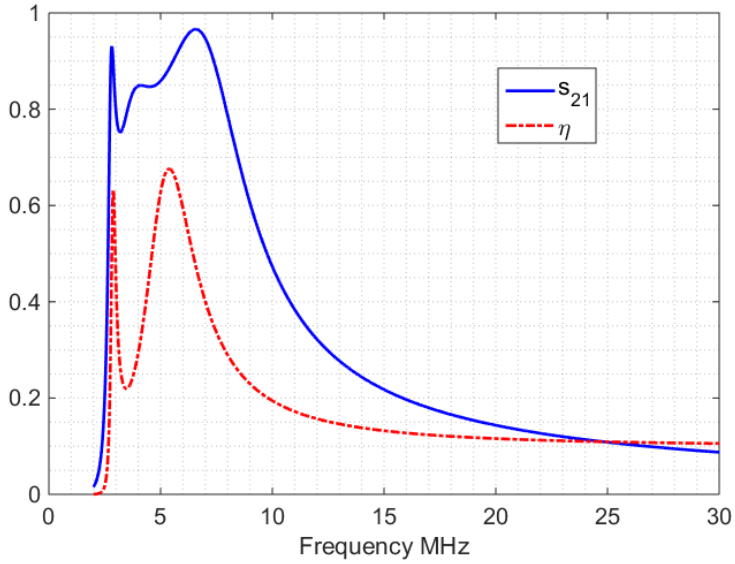

Figure 6. S_{21} and η curves for the solution in table III . S_{21} peak value is on the ISM band 6.78MHz.

Looking at Figure 5 and comparing the best result in terms of channel capacity as obtained in [27], which are relative to the reference design of table I, the improvement is evident: in [27] the maximum achievable channel capacity (depending on the S/N ratio) spans from 0.1 to 5 Mbit/s, while in this case C is included in the range between 4 and 60 Mbit/s.

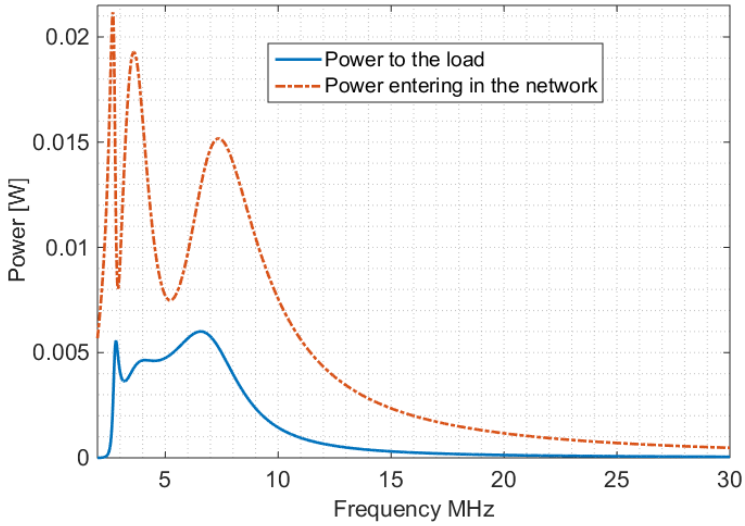

Figure 7. Input and output power of the WPT system for the solution in table III.

From the point of view of WPT, it is essential to verify the amount of power received. For this reason, we verified the amount of power entering in the network of Fig. 2 and the power received by the load. Figure 7 shows the power curves in the frequency domain, relative to the solution shown in figure 6. These curves represent the power values involved in the calculation of η in equation 16, where the input voltage is a sinusoid with an amplitude of 1 V_{rms}. The power reaching the load at 6.78MHz is 5mW, with a value of the η close to 0.5. The results shown in figures 6 and 7 are comparable, in terms of maximum S_{21} , η and power figures, to the results of the reference design represented by the parameters in table I. For comparison, in figures 8 and 9 we show the curves obtained using the reference design parameters. The benefit of the proposed design is then the increased broadband bandwidth and consequently the increased channel capacity as previously specified, also the proposed design does not sacrifice the power transfer figures.

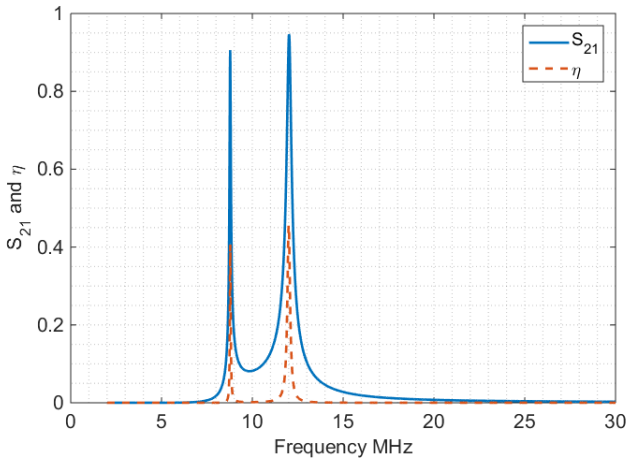

Figure 8. S_{21} and η curves for reference design solution of table I.

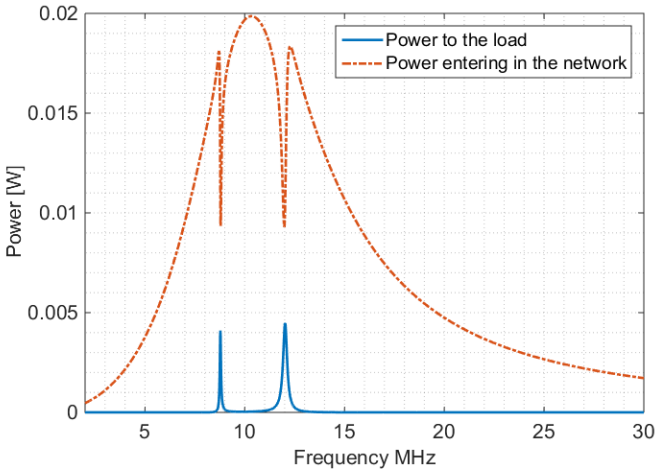

Figure 9. Input and output power of the reference WPT system model.

Figure 10 shows the Pareto front relative to this optimization run obtained both with SOC-MOP and the standard NSGA-II approach. The front obtained with our method completely dominates the points obtained with NSGA-II.

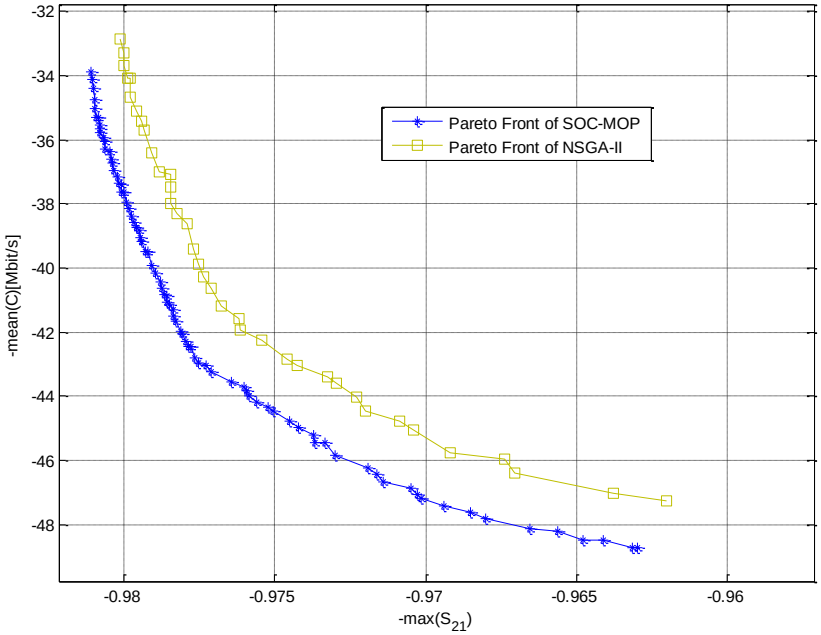

Figure 10. Pareto front with optimization performed on S_{21} and C, comparison with NSGA-II

Results for optimization of η and C

Figures 11 and 12 show the results obtained by optimizing the energy efficiency and the channel capacity; 70 different results have been obtained and, not as before, the curves are very different from each other. In particular, the energy efficiency curves can be roughly divided into three families, as indicated in Figure 11, characterized by

different maximum values of η and bandwidth. The same holds for the channel capacity which is characterized by higher variation.

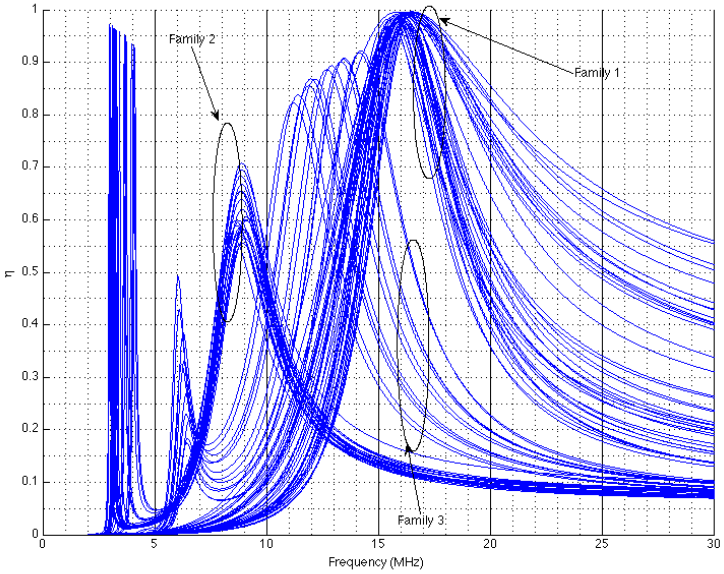

Figure 11. η curves with optimization performed on η and C

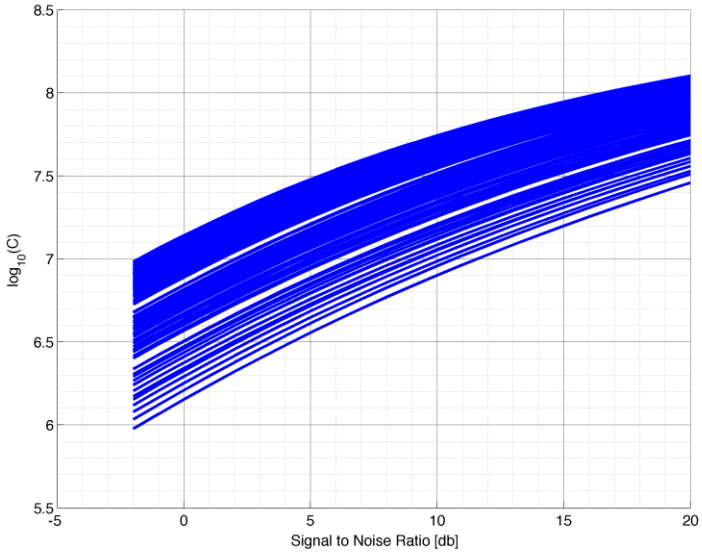

Figure 12. C curves with optimization performed on η and C

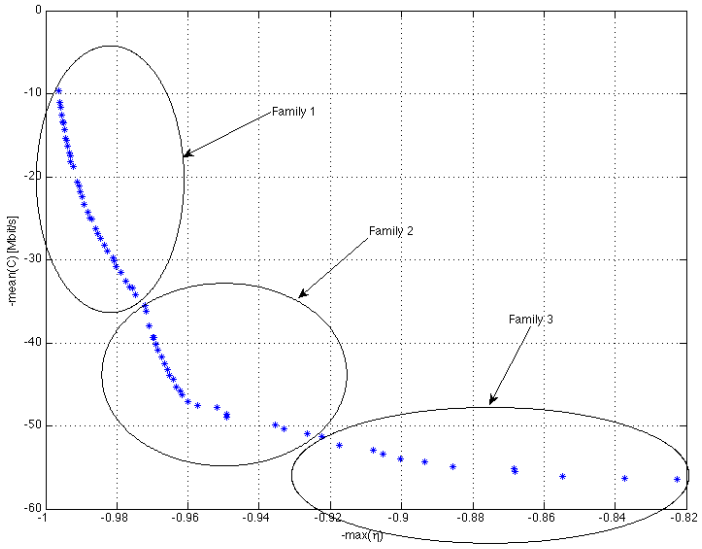

Figure 13. Pareto front with optimization performed on η and C

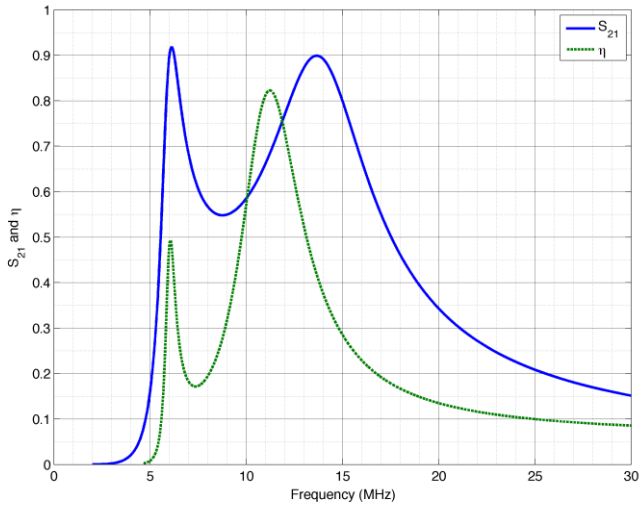

Figure 14. $S_{21}$and η curves with optimization performed on η and C

Figure 13 shows the corresponding Pareto front in which the points associated to the families of curves introduced in Figure 11 are also shown. The Pareto front obtained using NSGA-II is are not shown here, as the results are similar to those obtained in the previous case. It is now evident that wider bands (higher channel capacity) correspond to lower efficiency peaks and vice versa: the optimization procedure is in this case useful to choose the solution that fits the design goal, and the trade-off between the two desired objectives is now evident. Values of η very close to unity still have physical meaning (since the limits imposed on the parameters are based principally on physical meaning) but are related to extremely low values of parasitic resistances.

Figure 14 shows the power transfer efficiency and energy efficiency (when η and C are optimized) corresponding to the maximum achievable channel capacity (upper curve of Figure 12) which is in the range between 10 and 120 Mbit/s.

As a general comment on the results, looking at Figures 6 and 14, we can see that an efficiency peak (either relative to power transfer or to energy efficeincy) can be

selected and used for power transfer, while the remaining frequency spectrum can be used for data transfer. The results of both optimization runs lead to an increase of the channel capacity with respect to the nominal values of a regular WPT system.

Conclusions

This work presents a completely new algorithm for multi-objective optimization, that share a few points in common with a previously proposed algorithm for single objective optimization. The representative power of the topology preserving SOM neural network is used to create a new search strategy that heuristically shows good figures regarding exploitation, exploration and diversity preservation. Numerical results show that the proposed SOC-MOP algorithm is able to reach better results than the standard NSGA-II approach.

The proposed optimization method was used to optimize an analytical WPT system model both in terms of power and data transmission capabilities. The idea of using a WPT system as a channel for data communication, using an additive communication signal, is quite novel, and this work shows that even if a trade-off exists between channel capacity and channel energy efficiency (or transmitted power), a WPT system design is possible in order to obtain good figures in both fields. In fact, channel capacities of tens of Mbit/s can be achieved under a noisy scenario, simultaneously maintaining a good sub-channel for the power transfer signal.

With respect to existing optimal WPT design approaches, the multi-objective method presented in this work gives to the designer the flexibility to search and compare several optimal solutions, so that for instance the desired peak response is inside a desired frequency band, thus conceiving the desired response, and constraints, directly in the frequency domain. The optimization algorithm automatically finds feasible values of the lumped circuit parameters.

Regarding the objective of maximizing channel capacity, optimizing the channel in terms of efficiency produces channels with a larger band with respect to optimizing the transmitted power, then the system obtained has better characteristics for data transmission.

References

[1] Back, T.*Evolutionary Algorithms in Theory and Practice: Evolution Strategies, Evolutionary Programming, Genetic Algorithms*. New York: Oxford University Press. 1996

[2] Deb, K., et al. "A fast and elitist multiobjective genetic algorithm: NSGA-II." Evolutionary Computation, IEEE Transactions on 6.2 (2002): 182-197.

[3] Xiaodong L. "A non-dominated sorting particle swarm optimizer for multiobjective optimization." Genetic and Evolutionary Computation—GECCO 2003. Springer Berlin Heidelberg, 2003.

[4] Robič, Tea, and BogdanFilipič. "DEMO: Differential evolution for multiobjective optimization." Evolutionary Multi-Criterion Optimization. Springer Berlin Heidelberg, 2005.

[5] Barmada, S.,Raugi, M., andTucci, M."Global optimization algorithm based on self-organizing centroids," in *Evolutionary Computation (CEC), 2012 Congress on IEEE*,1-6, 2012

[6] Tucci, M., and Raugi, M, "Adaptive FIR Neural Model for Centroid Learning in Self-Organizing Maps".*IEEE Transactions on Neural Networks* 21: 948-960. 2010

[7] Tucci, M., and Raugi, M."A filter based neuron model for adaptive incremental learning of self-organizing maps". *Neurocomputing*: 74, 1815-1822. 2011
[8] Kohonen, T..*Self-Organizing Maps, Third Edition*. Berlin: Springer.2001
[9] A. Kurs, A. Karalis, R. Moffatt, J. Joannopoulos, P. Fisher, and M. Soljacic, "Wireless power transfer via strongly coupled magnetic resonances," Science, vol. 317, no. 5834, pp. 83-86, Jul. 2007.
[10] R. S. Y. Hui, W. Zhong, C. K. Lee, "A Critical Review of Recent Progress in Mid-Range Wireless Power Transfer", IEEE Transactions on on Power Electronics, Vol. 29, No. 9, September 2014
[11] Z. N. Low, R. A. Chinga, R. Tseng et. Al. "Design and Test of a High Power High Efficiency Loosely Coupled Planar Wireless Power Transfer System, " IEEE Transactions on Industrial Electronics, Vol. 56, No. 5, pp. 1801 – 1812, 2009.
[12] C. Huh, C. Park, C. T. Rim, S. Lee, G. H. Cho, "High performance inductive power transfer system with narrow rail width for On-Line Electric Vehicles" Proceedings of IEEE Energy Conversion Congress and Exposition (ECCE), 2010, pp. 647 – 651
[13] T. Imura, H. Okabe, Y. Hori, "Basic experimental study on helical antennas of wireless power transfer for Electric Vehicles by using magnetic resonant couplings", Proceedings of IEEE Vehicle Power and Propulsion Conference, 2009, pp. 936 – 940
[14] S. H. Lee, R. D. Lorenz, "Development and Validation of Model for 95%-Efficiency 220-W Wireless Power Transfer Over a 30-cm Air Gap", IEEE Transactions on Industry Application, vol. 47 no. 6, November/December 2011, pp. 2495 – 2504
[15] U. K. Madawala, D. J. Thrimawithana, "A Bidirectional Inductive Power Interface for Electric Vehicles in V2G Systems", IEEE Transactions on Industrial Electronics, vol. 56, no.10, October 2011, pp. 4789 – 4796
[16] M. Lienard, M. Carrion, V. Degardin, P. Degauque, "Modeling and Analysis of In – Vehicle Power Line Communication Channels, IEEE Transaction on Vehicular Technology, vol. 57 n.2, March 2008, pp. 670 – 679.
[17] V. Degardin, M. Lineard, P. Degauque, E. Simon, P. Laly, "Impulsive Noise Characterization of In – Vehicle Power Line", IEEE Transactions on EMC, vol 50 n. 4, November 2008, pp. 861 – 868.
[18] M. Mohammadi, L. Lampe, M. Lok, S. Mirabbasi, M. Mirvakili, R. Rosales, P. van Been, "Measurements Study and Transmission for In – vehicle Power Line Communication", ISPLC 2009, pp. 73 – 70.
[19] E. Bassi, F. Benzi, F. Almeida, T. Nolte "Powerline communication in electric vehicles" proceedings of Electric Machines and Drives Conference 2009, IEMDC 2009, p. 1749 – 1753.
[20] P. A. J. van Rensburg, H. C. Ferreira, A. J. Snyders "An Experimental Setup for In-Circuit Optimization of Broadband Automotive Power-Line Communications" ISPLC 2005, pp. 322- 325.
[21] N. Taherinejad, R. Rosales, S. Mirabbasi, L. Lampe, "A study on access impedance for vehicular power line communications," Power Line Communications and Its Applications (ISPLC), 2011 IEEE International Symposium on , vol., no., pp.440-445, 3-6 April 2011
[22] P. A. J. van Rensburg, H. C. Ferreira,A. J. Snyders, "An experimental setup for in-circuit optimization of broadband automotive power-line communications", Proceedings of IEEE ISPLC 2005, pp. 322 – 325.
[23] S. Barmada, L. Bellanti, M. Raugi, M. Tucci "Analysis of Power-Line Communication Channels in Ships.", IEEE Transactions on Vehicular Technology, Vol. 59, Issue 7, 2010, Pages 3161 – 3170

[24] S. Barmada, A. Musolino, M. Raugi, M. Tucci, “Analysis of Power Lines Uncertain Parameter Influence on Power Line Communications”, IEEE Trans. Power Delivery, Vol. 22, n. 4 pp. 2163 – 2171, October 2007
[25] S. Barmada, M. Raugi, M. Tucci, T. Zheng, “Power Line Communication in a Full Electric Vehicle: Measurements, Modelling and Analysis”, Proceedings of ISPLC 2010, Rio de Janeiro, Brazil, pp. 331 – 336.
[26] S. Barmada, M. Tucci, M. Raugi, Y. Maryanka, O. Amrani “PLC Systems for Electric Vehicles and Smart Grid Applications”, Proceedings of International Symposium on Power-Line Communications and Its Applications, ISPLC 213, 24 - 27 March, 2013, Johannesburg, South Africa, pp. 23 - 28
[27] S. Barmada, M. Raugi, M. Tucci, “Power line communication integrated in a Wireless Power Transfer system: A feasibility study”, Proceedings of International Symposium on Power Line Communications and its Applications (ISPLC 2014), Glasgow, UK, pp. 116 - 120
[28] Barmada, Sami, and Mauro Tucci. "Optimization of a magnetically coupled resonators system for Power Line Communication integration." Wireless Power Transfer Conference (WPTC), 2015 IEEE. IEEE, 2015.
[29] Inagaki, Naoki. "Theory of image impedance matching for inductively coupled power transfer systems." Microwave Theory and Techniques, IEEE Transactions on 62.4 (2014): 901-908.
[30] D.W.K. Ng, E. S. Lo, R. Schober, “Wireless Information and Power Transfer: Energy Efficiency Optimization in OFDMA Systems”, IEEE Trans. Wireless Commun., vol. 12, no. 12, pp. 6352 – 6370,. Dec. 2013.
[31] E.P. Caspers, S. H. Yeung, T. K. Sarkar, A. Garcia Lamperez, M. Salazar Palma, M. A. Lagunas, A. Perez Neira, “Analysis of Information and Power Transfer in Wireless Communications” IEEE Antennas and Propagation Magazine, vol. 55, no. 3, June 2014
[32] Besnoff, Jordan; Ricketts, David S., "Near field wireless power transfer and quadrature amplitude modulated (QAM) communication link," Wireless Power Transfer Conference (WPTC), 2015 IEEE , vol., no., pp.1,4, 13-15 May 2015
[33] P. Sample, D. A. Meyer, J. R. Smith, “Analysis, Experimental Results and Range Adaptation of Magnetically Coupled Resonators for Wireless Power Transfer”, IEEE Transactions on Industrial Electronics, vol. 58, no.2, February 2011, pp. 544 – 554.